Anisotropy of the Magnetocaloric effect: Example of Mn_5Ge_3

N. Maraytta[a,d], J. Voigt[a], C. Salazar Mejia[b], K. Friese[a,1], Y. Skourski[b], J. Perßon[a], S.M. Salman[c] and Th. Brückel[a,d].

[a]Jülich Centre for Neutron Science JCNS-2 and Peter Grünberg Institute PGI-4, Forschungszentrum Jülich GmbH, 52425 Jülich, Germany.

[b]Hochfeld-Magnetlabor Dresden (HLD-EMFL) Helmholtz-Zentrum Dresden-Rossendorf, 01328 Dresden, Germany.

[c]Physics Department, Al-Quds University, 90612 Abu Dis, Palestine.

[d]Lehrstuhl für Experimentalphysik IVc, RWTH Aachen University, 52056 Aachen, Germany.

Abstract

We have investigated the field direction dependence of the thermo-magnetic behavior in single crystalline Mn_5Ge_3. The adiabatic temperature change ΔT_{ad} in pulsed fields, the isothermal entropy change ΔS_{iso} calculated from static magnetization measurements and the heat capacity have been determined for field parallel and perpendicular to the easy magnetic direction [001]. The isothermal magnetization measurements yield furthermore the uniaxial anisotropy constants in second and fourth order, K_1 and K_2.

We discuss how the anisotropy affects the magneto-caloric effect (MCE) and compare the results to the related compound $MnFe_4Si_3$, which features an enhanced MCE, too, but instead exhibits strong easy plane anisotropy. Our study reveals the importance of magnetic anisotropy and opens new approaches for optimizing the performance of magnetocaloric materials in applications.

Keywords: Magnetocaloric effect, Mn_5Ge_3, pulsed magnetic fields, magnetic anisotropy, Heat capacity measurements.

Introduction

The interest in magnetic refrigeration as a new energy efficient and environmentally friendly solid-state cooling technology around room temperature has increased significantly in the last few years due to the concern about global warming and an ever-rising energy consumption. The magnetocaloric effect (MCE), which forms the basis of this refrigeration technology, is defined as the change of temperature (heating or cooling) and entropy of a magnetic material

[1]Corresponding author: Karen Friese k.friese@fz-juelich.de

due to a varying magnetic field **[1, 2, 3]**. This effect can be characterized quantitatively by the observed adiabatic temperature change (ΔT_{ad}) in an adiabatic process and by the entropy change (ΔS_{iso}) in an isothermal process **[4]**.

MCE investigations and applications use typically polycrystalline materials exhibiting large ΔT_{ad} or ΔS_{iso} **[5, 6, 7].** However, the magnetocrystalline anisotropy affects the magnetic susceptibility and consequently also the magnetocaloric effect, as the magnetic response is different for field along an easy direction or along a hard direction and the overall MCE will be the powder average. In an ideal polycrystalline material all crystallite orientations occur with identical probability and the temperature-dependent magnetic susceptibility of an ideal powder can be calculated from the weighted average of the magnetic susceptibilities of a single crystal as 1/3 of the value parallel to a certain axis and 2/3 of the value perpendicular to this axis. This relationship changes, if there is a stronger tendency for the crystallites in a powder to be oriented more in certain directions (e.g. due to shape anisotropy), and, as a consequence preferred orientation or texture arises. The presence or absence of preferred orientation should thus have a direct influence on the overall magnetic susceptibility and might be detrimental or advantageous for the size of the MCE.

The influence of the crystal field anisotropy on the MCE has been studied in the context of paramagnetic salts containing rare earth elements **[8]**. Many of the candidate materials for applications close the room temperature in the vicinity of a magnetic phase transition crystallize, however, in the hexagonal (e.g. materials related to Fe_2P **[9, 10]**, $La(Fe,Si)_{13}$ **[11, 12]** or MnAs **[13, 14]**) or tetragonal system (e.g. materials related to Mn_2Sb **[15]**), where anisotropy is inherently important due to the presence of one symmetry-salient direction. Investigations of anisotropy effects in these materials are scarce due to the fact that it is difficult to obtain most of these magnetocaloric materials as single crystals.

We have now succeeded to grow single crystals of the room temperature magnetocaloric compound Mn_5Ge_3. The compound crystallizes in the hexagonal space group $P6_3/mcm$ with lattice parameters a = 7.184(2) Å and c = 5.053(2) Å **[16]**. Within the structure, Mn occupies two different Wyckoff positions (Figure1 (left)) **[16, 17, 18].** The Mn1 atoms form an empty octahedron, while the Mn2 is incorporated at the center of [$Mn2Ge_6$]-octahedra.

Mn_5Ge_3 has a significant saturation magnetization M_s of 2.6(2) μ_B/Mn at 4 K **[19, 20]** and shows a presumably second order phase transition to a ferromagnetically ordered phase with observed Curie temperatures spreading from 290 to 304 K **[21-27].** The compound exhibits an easy axis anisotropy ‖[001] which was partly explained by magnetic dipolar interactions **[23].**

Spins on both Mn sites are aligned parallel to the hexagonal c-axis, yet magnetic moments on both sites differ significantly **[27, 16]** (Figure1 (right)). The magnetic entropy change of Mn_5Ge_3 measured on a polycrystalline sample shows a maximum value of 3.8 J/kg K for a

field change of 2 T **[22].** For samples in the shape of ribbons, a maximum value of 4.92 J/kg K was obtained for an external magnetic field of 3 T **[21].**

In this work, we study the magneto-caloric effect by means of indirect methods to determine ΔS_{iso} and ΔT_{ad} in Mn_5Ge_3 single crystals following the procedures described in the literature **[29-33]**. The direct measurements of the adiabatic temperature change (ΔT_{ad}) in pulsed magnetic fields will also be presented. Due to the short pulse duration, this technique provides nearly adiabatic conditions and the experimental conditions are close to the ones present in real applications **[34, 35].** In addition, they allow extracting information on the response time of the material and provide insight on the stability of a material when repeatedly exposed to a magnetic field. Taking advantage of the existence of large single crystals, we particularly focus our investigations on the elucidation of the direction dependence of the magnetocaloric effect in this compound. To this end, we also provide a detailed comparison to the closely related $MnFe_4Si_3$ which exhibits an easy plane anisotropy.

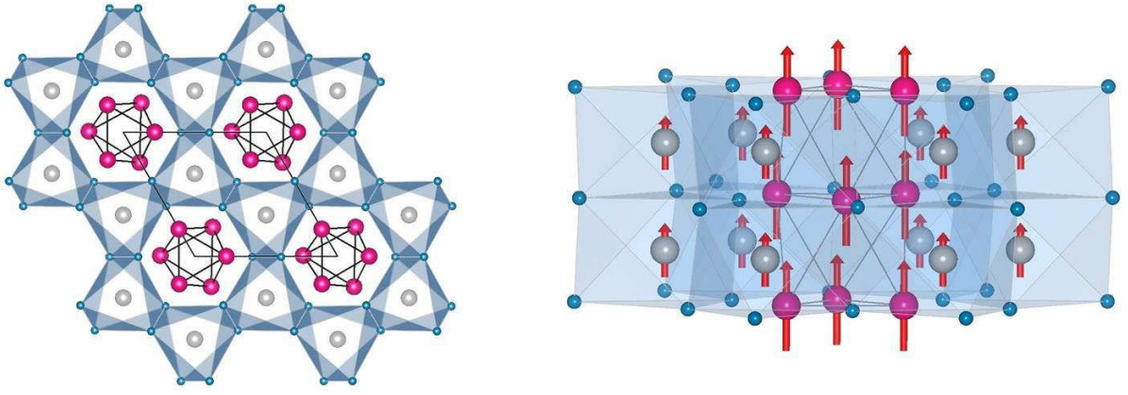

Figure 1. (Left) Projection of the structure of Mn_5Ge_3 in space group *P6₃/mcm* along the [001]-direction [36, 37, 16]. Sites occupied by Mn1 are shown in grey (*WP4d*), sites occupied by Mn2 are shown in pink (*WP6g*); Ge atoms are shown in blue (*WP6g*) and [$MnGe_6$]-octahedra are indicated also in blue. (Right) Schematic diagram illustrating the ferromagnetic structure of Mn_5Ge_3, projection slightly tilted from the [110]-direction. The length of the arrows corresponds to M = 1.96(3) μ_B and 3.23(2) μ_B for the *WP4d* and *WP6g* sites, respectively.

Experimental procedure

A single crystal of Mn_5Ge_3 was grown via the Czochralski Method from pre-synthesized polycrystalline material using stoichiometric amounts of the constituent elements (Mn 99.99% purity and Ge 99.9999% purity) according to the procedure described in **[38]**. The final crystal (diameter ≈1 cm, height ≈ 4cm) was oriented with a Laue camera and individual samples for heat capacity, magnetization measurements, as well as for the direct measurements of the magnetocaloric effect were cut by spark erosion. All samples were cut perpendicular to the hexagonal [001] and [100] crystallographic directions. X-ray powder diffraction on a ground piece of the single crystal confirmed the phase purity (Fig. S1).

The heat capacity data were collected using the thermal relaxation calorimeter of the PPMS Dynacool system in the temperature range from 2 to 395 K. For the measurements in zero

field, a low temperature apiezon N grease (Cryogenic High Vacuum Grease; 2 < T < 230 K) and a high temperature H grease (silicone-free high temperature vacuum grease; 210 < T < 395 K) were used. For the measurements in 1 and 2 T, the sample was fixed on the platform using silver paint to prevent the sample from moving and to ensure a good thermal contact between the sample and the platform. Due to the magnetic torque exerted on the sample, the measurement with the field parallel to the hard direction ([100] direction) was restricted to a maximum of 1 T (250 < T < 395 K). For each measurement point an addenda measurement was performed and subsequently subtracted.

Magnetization measurements were performed in static fields using a vibrating sample magnetometer (VSM) of Quantum Design PPMS. The external magnetic field was oriented perpendicular to the precut faces and isothermal magnetization curves were measured in the field range 9 T > $\mu_0 H$ > -0.1 T with different sweep rates, starting always from the maximum field at each temperature between 20 and 380 K. A demagnetization factor of N = 0.3394 was applied **[39]**. Temperature dependencies were derived from the isothermal magnetization measurements and compared to measurements under isofield conditions (B= 0.01 T and B= 0.5 T), for which the Maxwell relation

$$\left.\frac{\partial S}{\partial B}\right|_T = \left.\frac{\partial M}{\partial T}\right|_B$$

applies. From the data, $M(T)_B$ was extracted and the MCE was determined.

For the measurements with field parallel to the hard [100] direction, we plot H/M vs. M^2 (Fig.S2) to calculate the anisotropy constants K_1 and K_2 using the method introduced by Sucksmith and Thompson **[40]**.

Direct measurements of the magnetocaloric effect in pulsed magnetic field were performed at Dresden High magnetic field Laboratory by using their home-built experimental setup **[41]**.The measurements were performed with the field parallel to [100] and [001] directions up to 20 T and following the procedures described in **[42]**.

Results and discussion:

A. Heat capacity measurements

The analysis of $C_p(T)$ at low temperature yields the electronic specific heat coefficient γ= 51.1(1) mJ/mol K and a Debye temperature of Θ_D=509 (1) K. The heat capacity data in zero field show a well-developed λ-type peak at the magnetic Curie temperature (Figure 2). In applied magnetic field, the peak broadens and shifts towards higher temperatures. This observation corroborates the predominance of the ferromagnetic order (see Fig.S3 for the 2 T measurement in [001] direction). From the comparison we can see, that the application of a field of 1T reduces the heat capacity around the transition temperature more, if the field is applied ∥ [001]

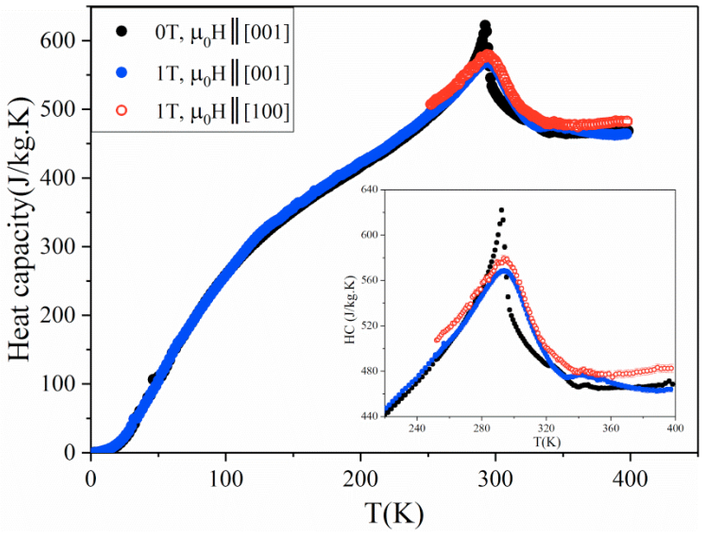

Figure 2. Temperature-dependent heat capacity data measured at 0 and 1 T with field parallel to [001] and at 1 T with the field parallel to [100] ([100] measurement - restricted to a max. field of 1 T and temperature range from 250 to 395 K due to the large magnetic torque exerted on the sample).

B. Magnetization measurement

We have measured the magnetic response using the high temperature option of the PPMS up to 1000 K. Only in the temperature range T > 550 K the susceptibility is proportional to 1/T and independent of the direction of the applied field indicating Curie-Weiss behavior. A fit of the Curie-Weiss law in the region T > 800 K (e.g. Fig. S4) yields a Curie constant of C = 1.1(1) $\times 10^{-4}$ m^3K/mol, Curie-Weiss temperature of 360(10) K and effective magnetic moment per transition metal ion μ_{eff} = 3.8(2) μ_B, i.e. the ordered moment as reported in **[28]** on the *WP*6*g* site at base temperature comes close to the effective paramagnetic moment per Mn, while the moment on the *WP*4*d* site is significantly smaller.

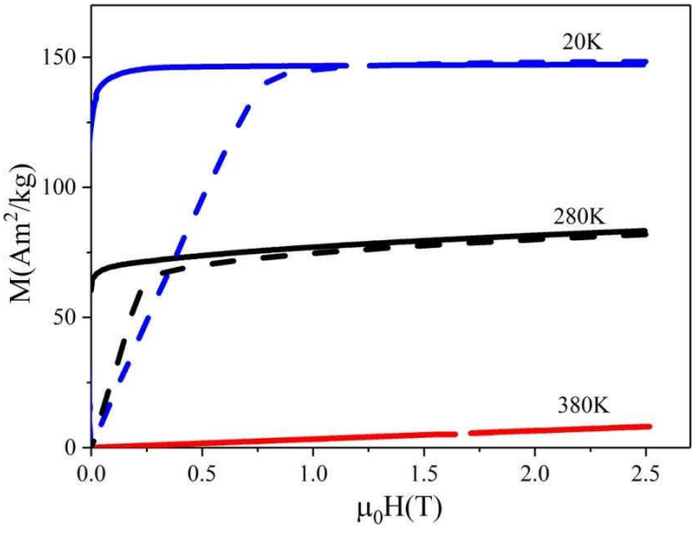

Figure 3: Selected Magnetization curves M(H) of Mn_5Ge_3 measured at different temperatures with the magnetic field applied along the [001]-direction (solid lines) and along the [100]-direction (dash lines).

The demagnetization corrected magnetization at different initial temperatures (Figure 3; see also Supplementary information, Fig.S5 for further M(H) curves) shows, that, along the easy [001] direction, saturation is reached at small fields < 0.3 T and only close to the transition temperature the field dependence broadens.

For the data with field parallel to the [100] direction, the response at small fields is lower. In the temperature range between T_C and 250 K the slope dM/dH is increasing with temperature, see Fig. S6. Below 250 K dM/dH remains nearly field and temperature independent below the anisotropy field H_a, which we identify as the locus of maximum curvature in the M(H) curves. Above H_a the magnetization for field parallel and perpendicular to the easy axis approach each other.

For the hexagonal system, second (K_1) and fourth order (K_2) anisotropy constants are considered for the anisotropy energy ($E_a = K_1\sin^2\theta + K_2\sin^4\theta$). θ is indicating the angle between the field and the easy direction. We applied the method introduced by Sucksmith and Thompson **[40]** to calculate the K_1 and K_2 from a plot of M^2 versus $\mu_0 H/M$. Before saturation is reached both observables have a linear relation and the slope yields K_2, while the y-axis intersection yields K_1+2K_2, as can be seen from a free energy expansion. At 20 K, we find the magnetic anisotropy constant $K_1 = 3.6(1)\times10^5$ J/m^3 (anisotropy field ≈ 0.8 T), while $K_2 = 1.3(1)\times10^4$ J/m^3. With further temperature increase, the anisotropy slowly decreases until approaching the Curie temperature $T_C \approx 296$ K (Figure 4). The results agree well with the ones in **[23]**.

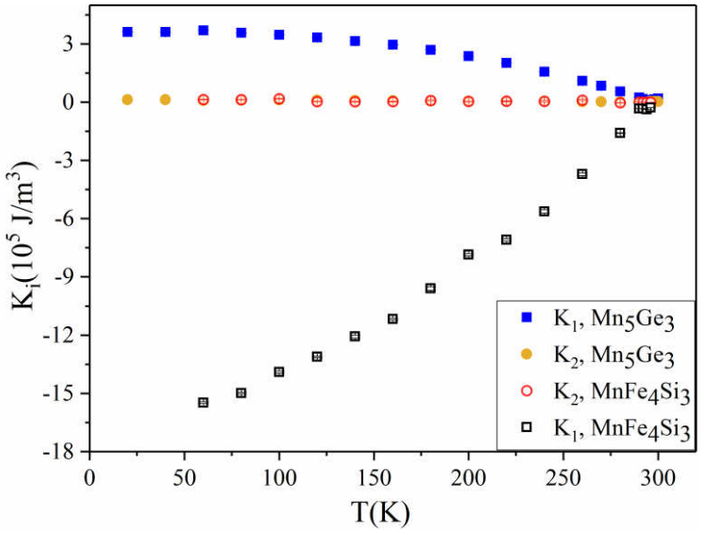

Figure 4. Temperature dependence of the magneto-crystalline anisotropy parameters for Mn_5Ge_3 and $MnFe_4Si_3$. The positive sign in K_1 of Mn_5Ge_3 is due to having an easy axis anisotropy meanwhile the negative sign for $MnFe_4Si_3$ is in line with an easy plane magnetic direction.

Thermal hysteresis loops of Mn_5Ge_3 showing the magnetization as a function of temperature at applied magnetic fields of 0.01 and 0.5 T parallel to [001] and [100] directions are presented in figure 5. The temperature dependent magnetic response shows hysteretic behavior of about 5 K along both directions (see the inset in figure 5 (a)) independent of the field direction and strength. The comparison between M(T) at 0.5 T from the isofield measurements and the ones extracted from the isothermal magnetization measurements- without demagnetization correction, green curves in figure 5- justifies the calculation of ΔS_{iso} from isothermal magnetization measurements, which is presented in figure 6 for different magnetic field changes ΔB.

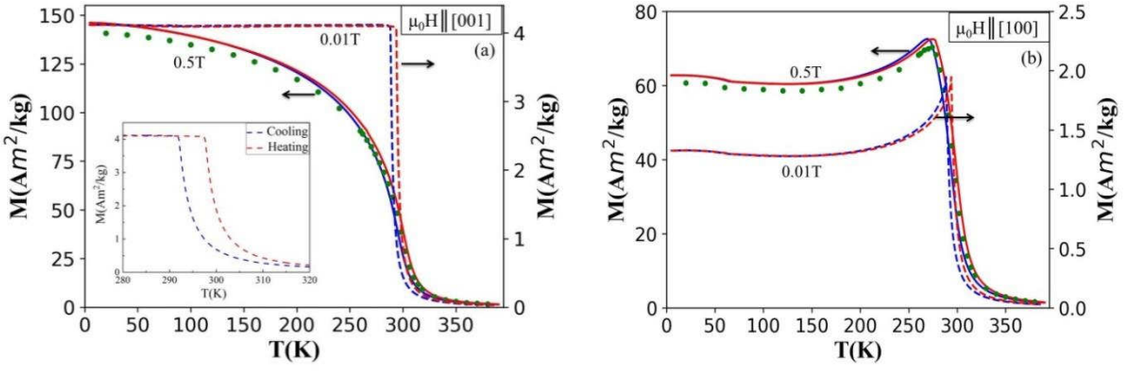

Figure 5. Temperature dependent magnetization of Mn_5Ge_3 at an applied field of 0.01 and 0.5 T in (a) [001] and (b) [100] directions. Lines are M(T) from isofield measurements and dots are $M(T)_B$ extracted from isothermal measurements. Inset shows the magnetic transition region at 0.01 T ‖ [001].

ΔS_{iso} features the maximum at 296 K for both field directions. The entropy change for the easy and hard direction differs by 0.4 J/kg.K for all three ΔB (see figure 6, black closed symbols for $\mu_0H \| [001]$ and red open symbols for $\mu_0H \| [100]$). The difference vanishes for

temperatures sufficiently higher than the transition temperature. Below T_C the anisotropy of the effect is quite present and it is more pronounced at lower fields. Below the transition temperature, the respective average of these values is consistent with the earlier results from a polycrystalline sample **[22, 25]** and the results from the sample in form of ribbons- unfortunately, no information about the orientation of the ribbons is given in the article, so that a more detailed comparison regarding the anisotropy is not feasible **[21]**.

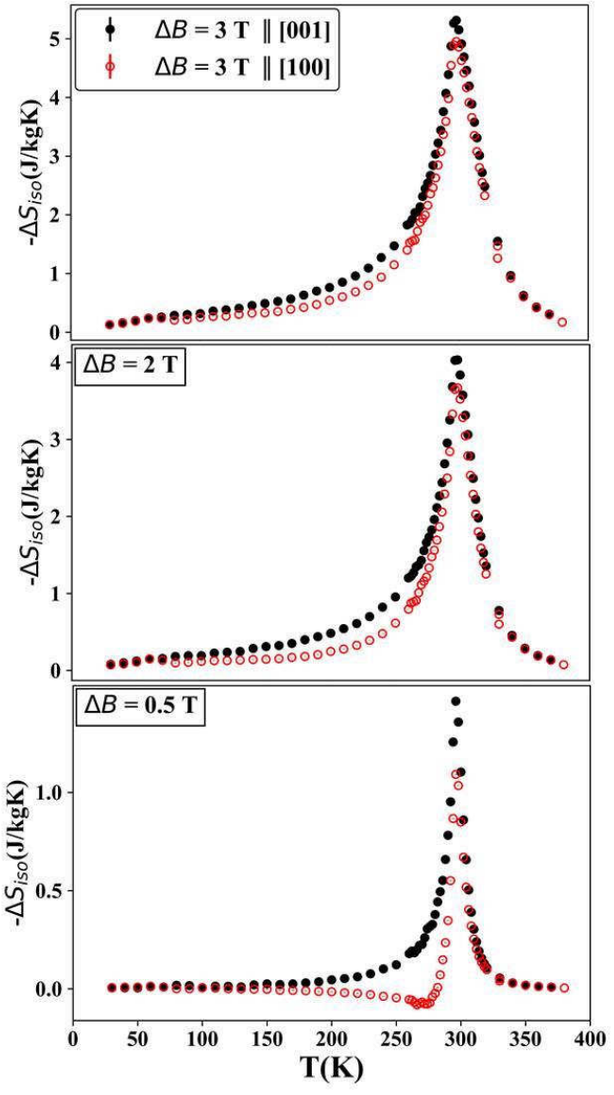

Figure 6. Magnetic entropy change of Mn_5Ge_3 determined from magnetization data at a field of 0.5, 2 and 3 T parallel to [001] (black closed symbol) and [100] (red opened symbol) directions.

When a small field < 1.2 T is applied along the [100] direction, a small inverse MCE is observed between 150 and 290 K, i.e. the entropy increases with increasing field (blue area in the right panel of figure 7) due to the fact that the small magnetic field cannot overcome the anisotropy. With further increase of temperature, the anisotropy decreases and smaller fields are sufficient to align the moments with the field. As a consequence, the entropy changes the sign and increases stronger than linear with field. A similar behavior was also observed in the

compound $MnFe_4Si_3$ which is isostructural to Mn_5Ge_3, yet exhibits mixed occupancy of Mn and Fe on the *WP*6*g* site and a ferromagnetic structure with the spins aligned in the *a,b*-plane **[42]**.

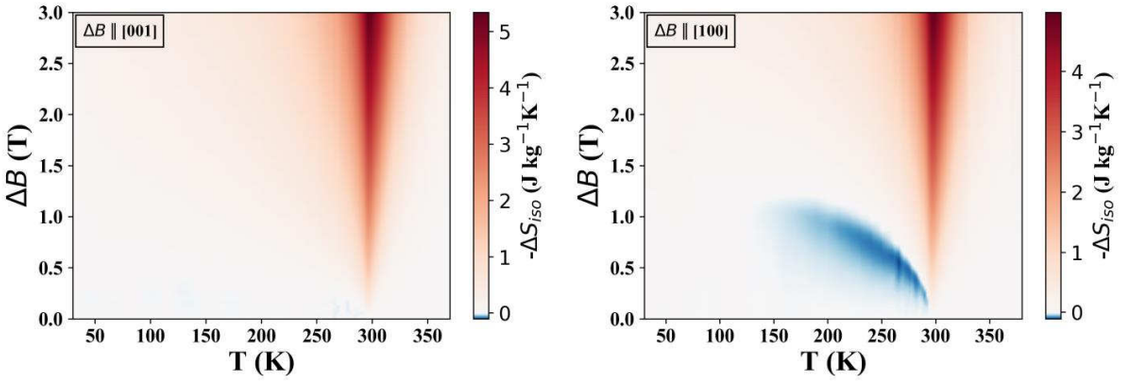

Figure7. Colour plot of the magnetic entropy change of Mn_5Ge_3 as a function of temperature and magnetic field change parallel to [001] and [100]. Blue colours indicate a positive ΔS_{iso} and hence an inverse MCE, red colours correspond to a negative ΔS_{iso} and hence normal MCE.

C. Direct measurement of ΔT_{ad}

To probe the applicability of the material on the time scale close to that of possible applications we performed direct measurements of ΔT_{ad} in pulsed fields. For that we record the temperature of the sample as the field is ramped in ~50 ms to 2 T and 20 T.

The ΔT_{ad} values are obtained by processing the signal from the thermocouple, one joint of which is connected to the sample. A lot of effort is put in order to minimize the thermalization time and to cancel the contributions induced in the leads by the time dependent variation of the magnetic field and sample magnetization. Figure 8 presents the as-recorded data measured for the two directions –easy and hard directions- at 297.5 K in 2 T pulses (see Fig.S7 for the data at 300 K). The upper graphs show the time dependencies of the magnetic field and the thermocouple response. Here the thermocouple signal resembles the pulse profile rather tightly, indicating a reasonably good coupling to the sample. More thorough test of the coupling is the field dependence of ΔT_{ad}. The lower graphs show the temperature changes replotted against the field. Here the finite response time shows up as an opening of the curve upon up- and down-sweeps. The difference in shape of the field dependencies between the two directions reflect the thermal contact quality between the particular directions, which is also seen by the lagging of the temperature signal behind the field signal. A similar behavior is seen for 20 T pulses shown in Fig.S8.

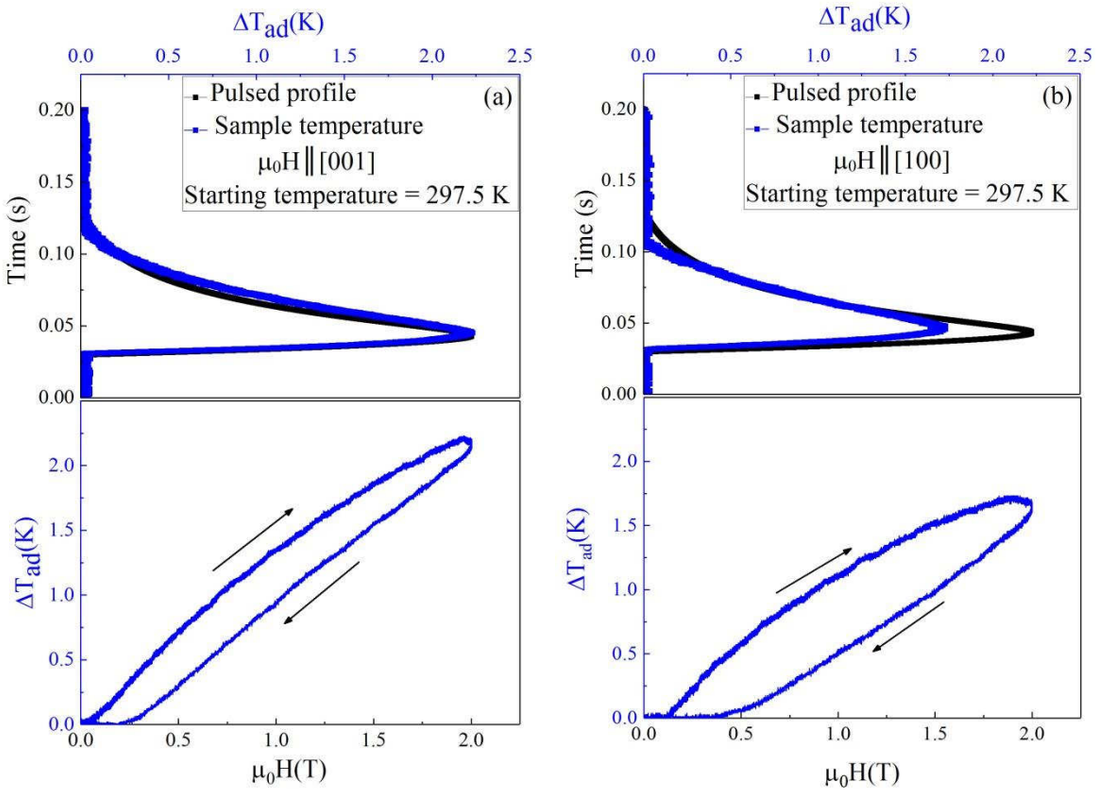

Figure 8. Field and time dependence of ΔT_{ad} for a pulsed magnetic field of 2 T applied along the [001] direction (a) and along the [100] direction (b) at 297.5 K.

The adiabatic temperature change reaches different maximum values along the easy and the hard direction (Figure 9 (a)); ≈ 2.3(1) K for H‖[001] at 295 K as compared to ≈ 2.0(1) K for H‖[100] at 300 K in pulsed magnetic fields of 2 T. These values are in agreement with the values calculated from the isothermal entropy change and the specific heat measurements (details in Fig. S9). The observations show that i) this material is quite capable of transferring heat on the time scale of about 15 ms, and ii) that at least at the top of the pulse corresponding to the maximum values the data are quite reliable. With that stated, we have extended the field range up to 20 T (Figure 9 (b), Fig. S8) where the the observed peak broadens and shifts to higher temperatures, ΔT_{ad} differs also by ~ 10% for the two directions; ≈ 10.8(2) K for H‖[001] at 305 K as compared to ≈ 9.8(4) K for H‖[100] at 310 K. ΔT_{ad} varies roughly as $H^{2/3}$, as expected for localized ferromagnetism at T_C **[43]**.

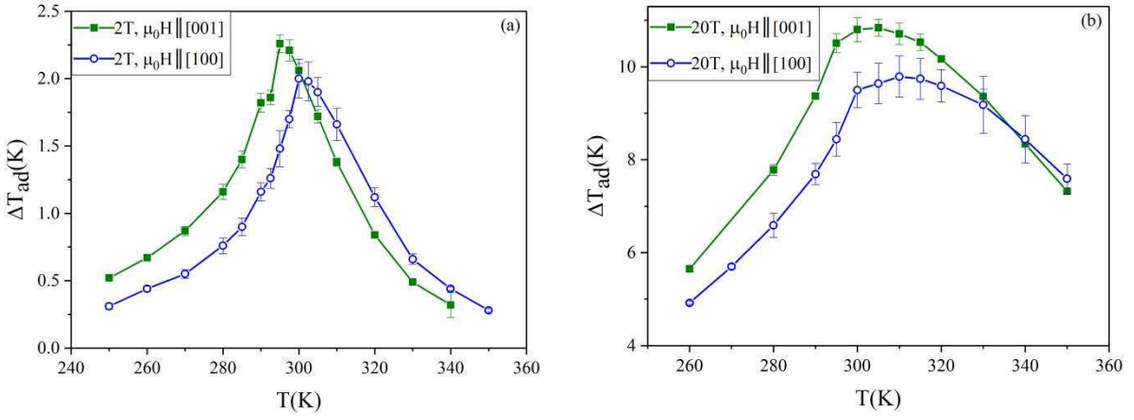

Figure 9. Comparison of ΔT_{ad} measured in pulsed magnetic fields of 2 T (a) and 20 T (b) with the field parallel to [001] and [100]. The lines drawn in the figures are just to guide the eyes. Comparison of ΔT_{ad} measured in pulsed magnetic fields and calculated from heat capacity in static magnetic fields of 2 T is given in the supplement (Fig. S9).

D. Comparison to relevant compounds

It is intriguing to compare Mn_5Ge_3 with the isostructural Mn_5Si_3 **[44, 45]** which has also been widely studied for its magnetic and magnetocaloric properties. However, Mn_5Si_3 orders antiferromagnetically at much lower temperature and exhibits an inverse MCE related to a phase transition between two antiferromagnetic structures. Yet the isostructural compound $MnFe_4Si_3$ where the *WP*4*d* site is mainly occupied by Fe while the *WP*6*g* site has mixed occupancy of Mn and Fe provides an ideal point of comparison: it orders ferromagnetically with a T_C close to 300 K and a normal MCE **[38, 42]**. The main magnetic characteristics of both compounds are given here:

Table I. Comparison between the main magnetic characteristics of Mn_5Ge_3 and $MnFe_4Si_3$ compounds.

Mn_5Ge_3	**$MnFe_4Si_3$ [38,42]**
Easy axis *c* ([001])	Easy plane *a,b*
Moment *WP*6*g* site: 3.23(2) μ_B **[28]**	*WP*6*g* site: 1.5(2) μ_B
Moment *WP*4*d* site: 1.96(3) **[28]**	*WP*4*d* site: 1.1(12)μ_B[2]
ΔS_{iso} = 2.5 J/kg.K (1 T ∥ [001])	ΔS_{iso} = 1.3 J/kg.K (1 T ∥ [100])

[2] The refined magnetic moment in the M2 sites are not larger than the corresponding standard deviation and therefore were not taken into account in the refinement **[38].**

ΔS_{iso} = 2.15 J/kg.K (1 T⊥ [001])	ΔS_{iso} = 0.47 J/kg.K (1 T⊥ [100])
ΔT_{ad} = 2.3(1) K (2T ‖ [001])	ΔT_{ad} = 1.38(1) K (2T ‖[100])
ΔT_{ad} = 2.0(1) K (2T ⊥ [001])	-
$K_1 = 3.7(1)\times10^5$ J/m^3 (60 K)	$K_1 = -1.5(1)\times10^6$ J/m^3 (60 K)^3

In difference to Mn_5Ge_3 where the spins are aligned along *c* ([001]), the spins in $MnFe_4Si_3$ are aligned in the *a,b* plane **[38, 42]**. In both compounds the magnetic moment on the *WP*6*g* site is larger than on the *WP*4*d* site, in $MnFe_4Si_3$ it was even not possible to refine any ordered moment for the *WP*4*d* site[2].

Mn_5Ge_3 has small magnetic anisotropy (K_1= 3.7(1)×10^5 J/m^3 at 60 K) with *c* being the easy axis, while $MnFe_4Si_3$ shows a much larger magnetic anisotropy (see Figure 4). Provided an ideal powder is used in applications, the large anisotropy of $MnFe_4Si_3$ could therefore limit the size of the MCE in this compound (and other compounds with similar characteristics) when compared to the MCE in a single crystal, while for Mn_5Ge_3 (and similar compounds) the reduction of the MCE will be comparatively weak. On the other hand, the targeted introduction of preferred orientation might also be beneficial for increasing the MCE in materials with large anisotropy and might represent a new approach for optimizing their performance.

Conclusions

The anisotropy of the magnetocaloric properties in Mn_5Ge_3 was studied in static and pulsed magnetic fields. The uniaxial magnetic anisotropy decreases with temperature and can be overcome by applied fields $\mu_0H > 0.8$ T; the anisotropy constants are calculated over a broad temperature range up to second order. The comparison with $MnFe_4Si_3$, which exhibits an easy plane anisotropy shows, that in Mn_5Ge_3, the dependence of the size of the MCE on the field direction is less pronounced. However, despite the fact that anisotropy constants vanish towards T_C, the MCE in Mn_5Ge_3 features also a significant anisotropy that is seen in the adiabatic temperature change in pulsed field and also in the isothermal entropy change.

This study suggests that the magnetic anisotropy should be taken into account when trying to optimize the performance of magnetocaloric materials. In applications, the control of preferred orientation and texture, depending on the specific anisotropic characteristics of the candidate materials, could be beneficial for increasing the size of the magnetocaloric effect.

[3] Figure 4, based on M(H) in **[42]** compared to -2.8×10^6 J/m^3 at 50 K in **[46]**, the difference is due to a slightly different Fe content ($Mn_{\sim0.86}Fe_{\sim4.24}Si_{\sim2.90}$ in **[46]**).

Journal of Applied Physics

AIP Publishing

Supplementary Material

See Supplementary Material for more information about the anisotropy calculation, heat capacity measurements, Curie Weiss fit, isothermal magnetization curves with dM/dH calculation and for more details about the pulsed field measurements with a comparison of the results (ΔT_{ad}) with the ones obtained from the static field measurements.

Acknowledgements

This work is part of a collaborative agreement between the Forschungszentrum Jülich and Al-Quds University and was supported by the BMBF under the programme *Zusammenarbeit mit Entwicklungs- und Schwellenländern im Nahen Osten, Nordafrika, Türkei* (Project MagCal, 01DH17013) and under the Joint Research and Education Programme *Palestinian German Science Bridge PGSB.* The work is based upon experiments performed at HLD at HZDR, member of the European Magnetic Field Laboratory (EMFL). We would like to thank Lukas Berners for the XRD measurements.

Data availability

The data that support the findings of this study are available from the corresponding author upon reasonable request.

References

[1] K.A. Gschneidner Jr. and V.K. Pecharsky, *Int. J. Refrig.* **31**, 945 (2008).

[2] C.B. Zimm, A. Jastrab, A. Sternberg, V. Pecharsky, K.A. Geschneidner Jr., M. Osborne and I. Anderson, *Adv. Cryogenic Engineering* **43**, (1998).

[3] B.F. Yu, Q. Gao, B. Zhang, X.Z. Meng and Z. Chen, *Intl. J. Refrig.* **26**, 622 (2003).

[4] A. Kitanovski and P.W. Egolf, *Int. J. Refrig.* **29**, 3 (2006).

[5] C.F. Sánchez-Valdés, R.R. Gimaev, M. López-Cruz, J.L. Sánchez Llamazares, V.I. Zverev, A.M.Tishinc, A.M.G. Carvalho, D.J.M. Aguiar, Y. Mudryk and V.K. Pecharsky, *J. Magn. Magn. Mater*. **498**, 166130 (2020).

[6] A. O. Guimarães, M. E. Soffner, M. Mansanares, A. A. Coelho, A. Magnus G. Carvalho, M. J. M. Pires, S. Gama and E. C. da Silva, *J. Appl. Phys.***107,** 073524 (2010).

[7] K. Fukamichi, A. Fujita and S. Fujieda, *J. Alloys Compds.* **408–412**, 307 (2006).

[8] M. D. Kuz'min and A. M. Tishin, *J. Phys. D: Appl. Phys* **24**, 2039 (1991).

[9] N.T. Trung, Z.Q. Ou, T.J. Gortenmulder, O. Tegus, K.H.J. Buschow and E. Brück, *Appl. Phys. Lett.* **94**, 102513 (2009).

[10] O. Tegus, E. Brück, K.H.J. Buschow and F.R. de Boer, *Nature (London)* **415**, 150 (2002).

[11] F.X. Hu, B.G. Shen , J.R. Sun, Z.H. Cheng, G.H. Rao and X.X. Zhang, *Appl. Phys. Lett.***78**,3675 (2001)

[12] A. Fujita, S. Fujieda, Y. Hasegawa and K. Fukamichi, *Phys. Rev.* **B67,** 104416 (2003).

[13] H. Wada and Y. Tanabe, *Appl. Phys. Lett.***79,** 3302 (2001).

[14] P.F. Xu, S.H. Nie, K.K. Meng, S.L. Wang, L. Chen and J. H. Zhao, *Appl. Phys. Lett.***97**, 042502 (2010).

[15] S.C. Ma, D. Hou, Y.Y. Gong, L.Y. Wang, Y.L. Huang, Z.C. Zhong, D.H. Wang and Y. W. Du, *Appl. Phys. Lett.* **104**, 022410 (2014).

[16] R. Ciszewski, *phys. stat. sol.* **3**, 1999 (1963).

[17] G. Kappel, G. Fischer, and A. Jaegle, *phys. stat. sol. (a)* **34**, 691 (1976).

[18] D.H. Day and R.N. Sinclam, *Acta Crystallogr.* **B26**, 2079 (1970).

[19] G. Kappel, G. Fischer and A. Jaegle, *Phys. Lett.* **45**, 3 (1973).

[20] X.B. Liu and Z. Altounian, *J. Appl. Phys.* **99**, 08Q101 (2006).

[21] T.F. Zheng, Y.G. Shi, C.C. Hu, J.Y. Fan, D.N. Shi, S.L. Tang and Y.W. Du, *J. Magn. Magn. Mater.* **324**, 4102 (2012).

[22] Songlin, Dagula, O. Tegus, E. Brück, F.R. de Boer and K.H.J. Buschow, *J. Alloys Compds* **337**, 269 (2002).

[23] Y. Tawara and K. Sato, *J. Phys. Soc. Jpn.* **18**, 773 (1963).

[24] F.Q. Zhao, W. Dagula, O. Tegus and K.H.J. Buschow, *J. Alloys Compds.* **416**, 43 (2006).

[25] T. Tolinski and K. Synoradzki, *Intermetallics* **47**, 1 (2014).

[26] K.H. Kang, J.H. Kim, J.W. Kim, K.C. Chung and C.S.Yoon , *J. Alloys Compds.* **729**, 603 (2017).

[27] Y. Kim, K.H. Kang, J. H. Kim, E.J. Kim, K. Choi, W.B. Han, H.S. Kim, Y. Oh and C.S. Yoon, *J. Alloys Compds.* **644**, 464 (2015).

[28] J.B. Forsytht and P.J. Brown, *J. Phys.: Condens. Matter* **2**, 2713 (1990).

[29] V.K. Pecharsky and K.A. Gschneidner Jr., *J. Appl. Phys.* **85**, 5365 (1999).

[30] M. Foldeaki, R. Chahine, and T.K. Bose, *J. Appl. Phys.* **77**, 3528 (1995).

[31] K. A. Gschneidner and Jr. and V. K. Pecharsky, *Annu. Rev. Mater. Sci.* **30**, 387 (2000).

[32] V. K. Pecharsky and K. A. Gschneidner Jr., *J. Appl. Phys.* **86**, 565 (1999).

[33] V.K. Pecharsky, K. A. Gschneidner, Jr., A. O. Pecharsky, and A. M. Tishin, *Phys. Rev. B* **64**, 144406 (2001).

[34] J. Liu, T. Gottschall, K. P. Skokov, J. D. Moore, and O. Gutfleisch, *Nat. Mater.* **11**, 620 (2012).

[35] F. Cugini, G. Porcari, C. Viappiani, L. Caron, A.O. dos Santos, L.P. Cardoso, E.C. Passamani, J.R. C. Proveti, S. Gama, E. Brück, and M. Solzi, *Appl. Phys. Lett.* **108**, 012407 (2016).

[36] C. Salazar-Mejía, V. Kumar, C. Felser, Y. Skourski, J. Wosnitza and A.K. Nayak, *Phys. Rev. Appl.* **11**, 054006 (2019).

[37] P. Devi, M. Ghorbani Zavareh, C. Salazar Mejía, K. Hofmann, B. Albert, C. Felser, M. Nicklas and Sanjay Singh, *Phys. Rev. Mater.* **2**, 122401 (2018).

[38] P. Hering, K. Friese, J. Voigt, J. Perßon, N. Aliouane, A. Grzechnik, A. Senyshyn and T. Brückel, *Chem. Mater.* **27**, 7128 (2015).

[39] D.X. Chen, E. Pardo and A. Sanchez, *IEEE Trans. Magn.* **38**, 4 (2002).

[40] W. Sucksmith, F.R.S. Thompson and J.E. Thompson, *Proc. Royal Soc.* **A 225**, 362 (1954).

[41] M. Ghorbani Zavareh, C. Salazar Mejía, A. K. Nayak, Y. Skourski, J. Wosnitza, C. Felser and M. Nicklas, *Appl. Phys. Lett.* **106**, 071904 (2015).

[42] N. Maraytta, Y. Skourski, J. Voigt, K. Friese, M. G. Herrmann, J. Perßon, J. Wosnitza, S. M. Salman and T. Brückel, *J. Alloys Compds.* **805**, 1161 (2019).

[43] H. Oesterreicher and F. T. Parker, *J. Appl. Phys.* **55**, 4334 (1984).

[44] M. Gottschilch, O. Gourdon, J. Perßon, C. de la Cruz, V. Petricek, and T. Brückel, *J. Mater. Chem.* **22**, 15275 (2012).

[45] G. Kappel, G. Fischer and A. Jaegle, phys. stat. sol. **34**, 691 (1976).

[46] H. Yibolea, W. Hanggaia, Z.Q. Oua, R. Hamaneb, V. Hardyb and F. Guilloua, *J. Magn. Magn. Mater* **504**, 166597 (2020).

AIP Publishing

Journal of Applied Physics

ACCEPTED MANUSCRIPT

PLEASE CITE THIS ARTICLE AS DOI: 10.1063/5.0020780

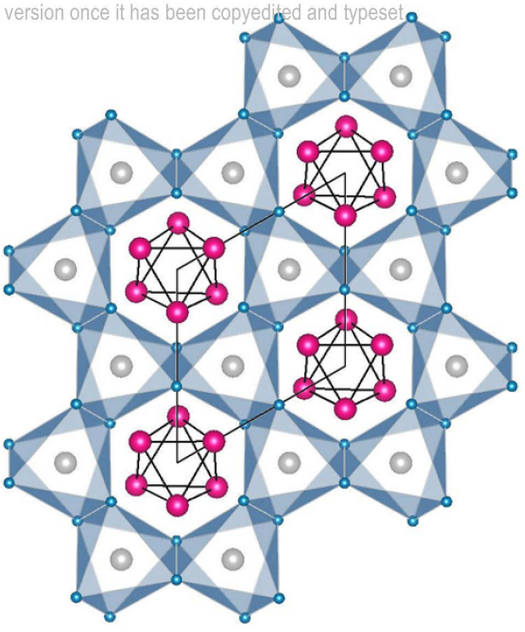

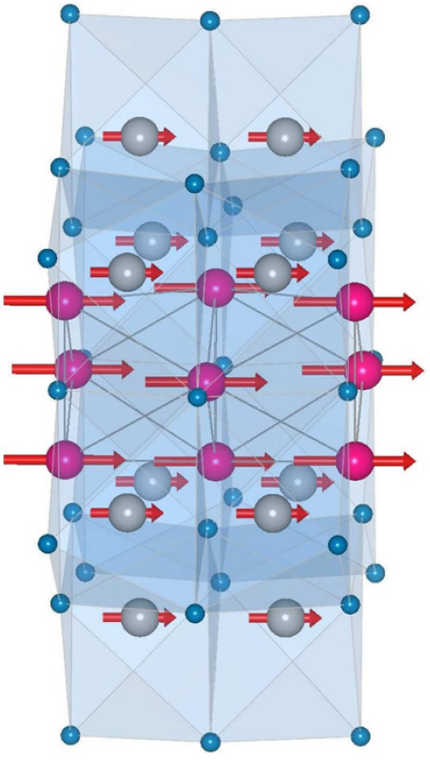

Journal of Applied Physics

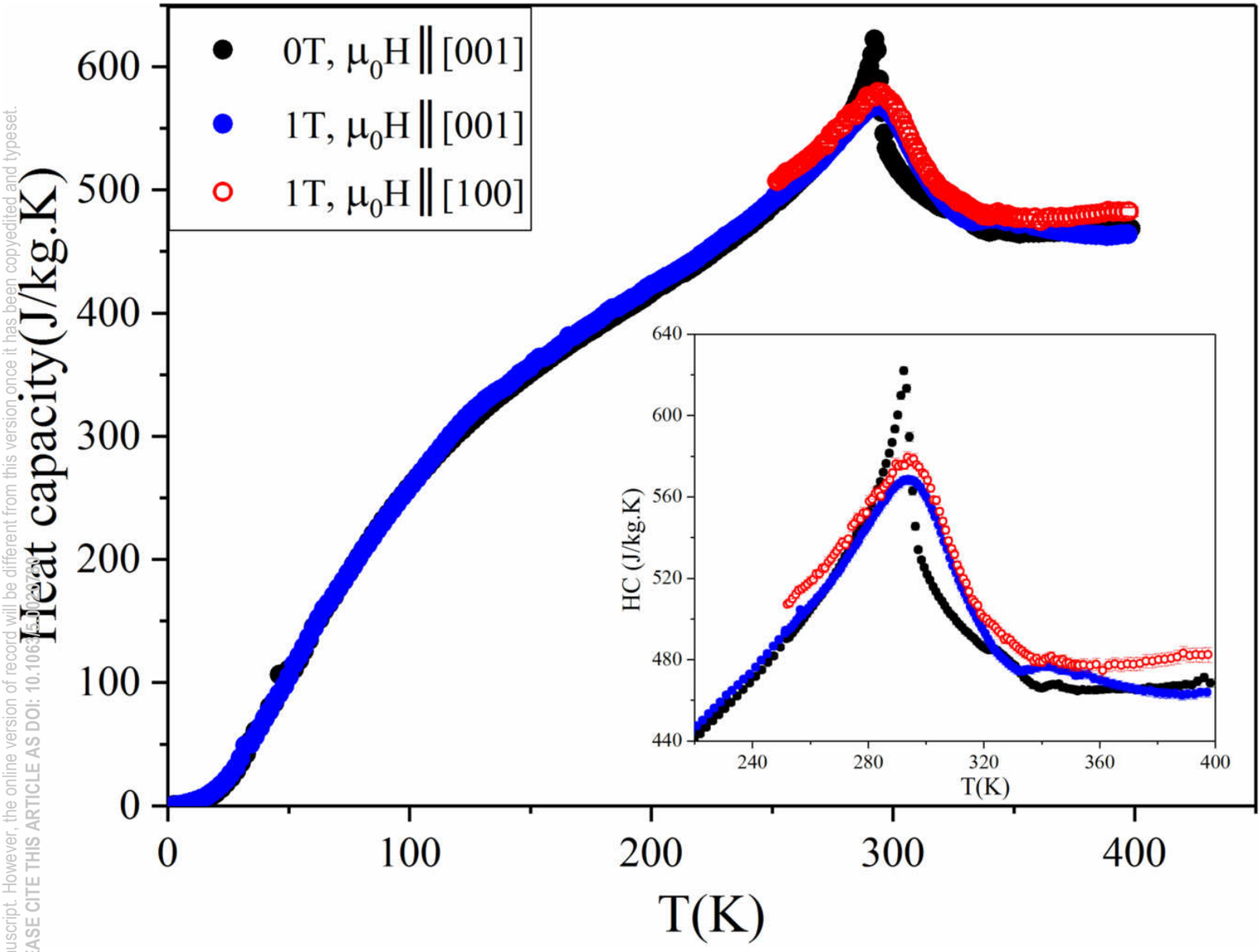

Journal of Applied Physics

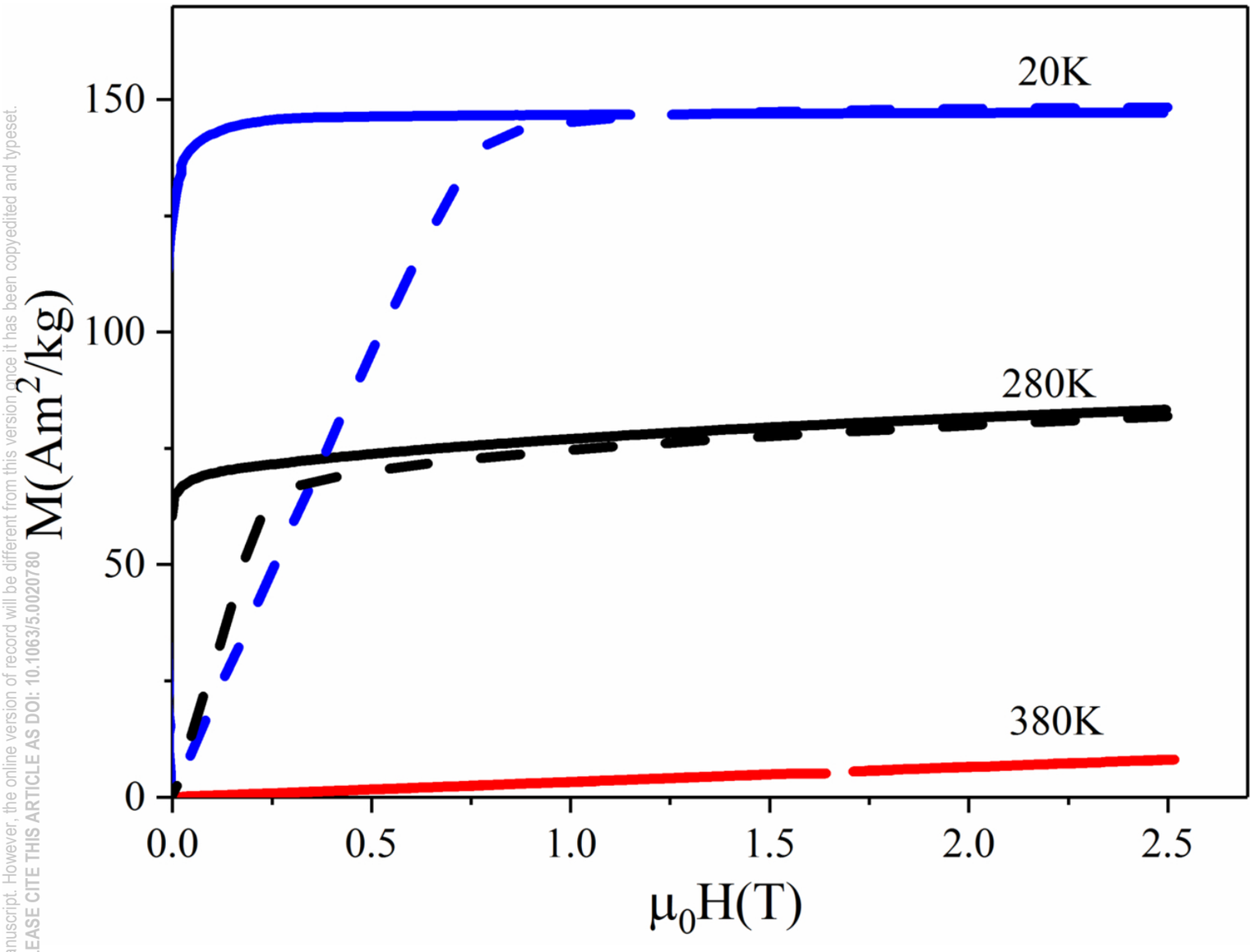

AIP Publishing

Journal of Applied Physics

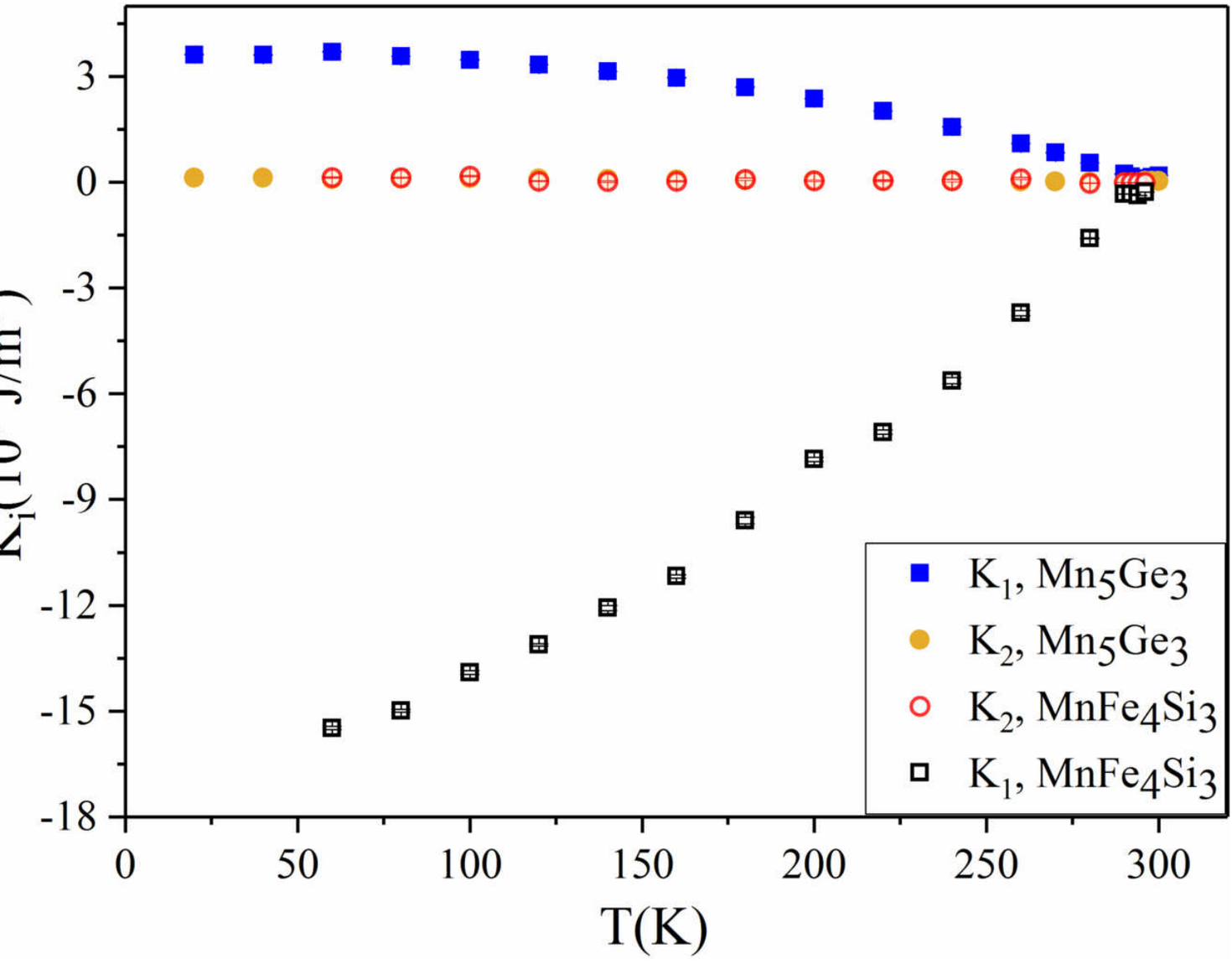

AIP Publishing

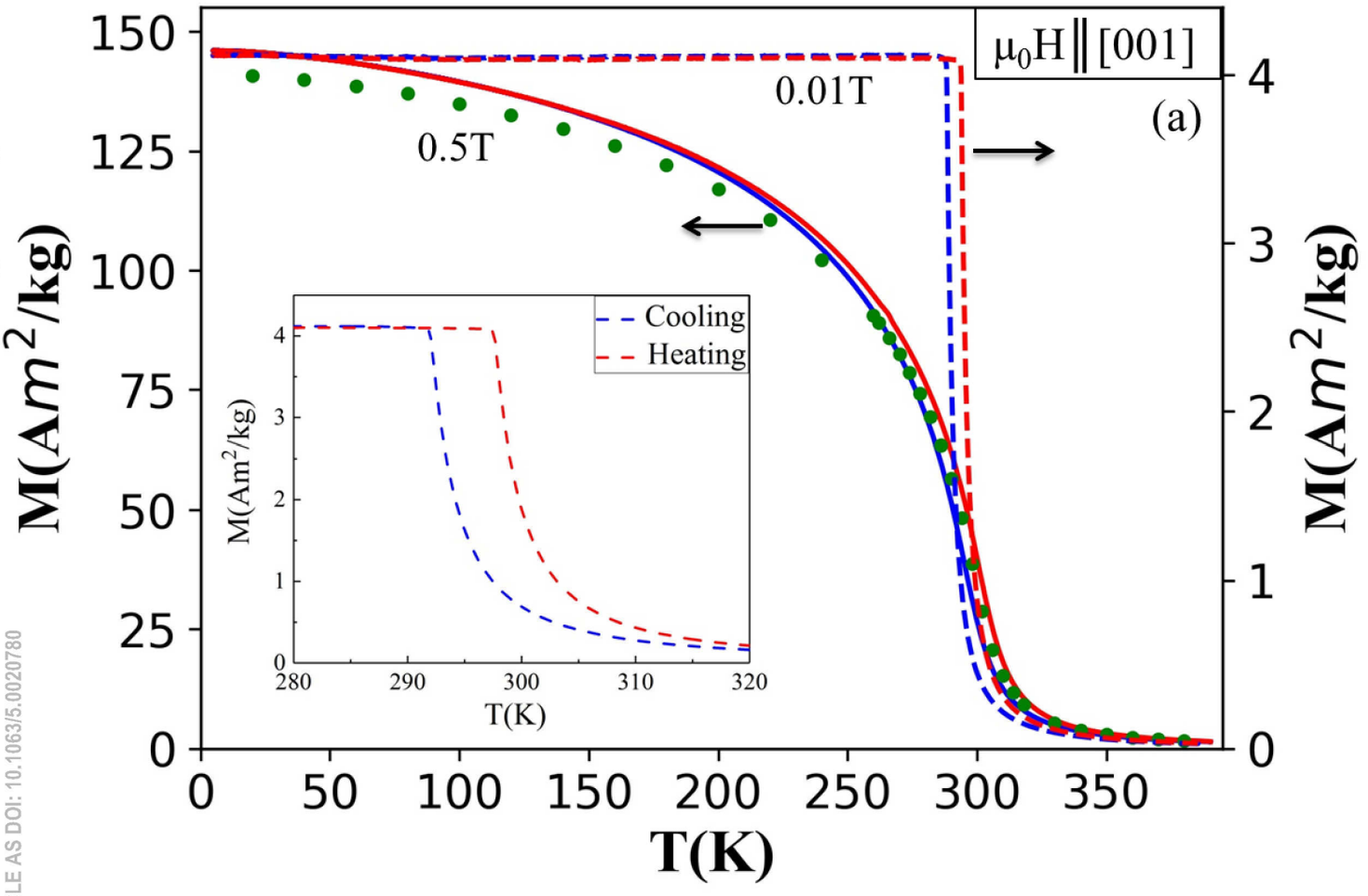

AIP Publishing
Journal of Applied Physics

PLEASE CITE THIS ARTICLE AS DOI: 10.1063/5.0020780

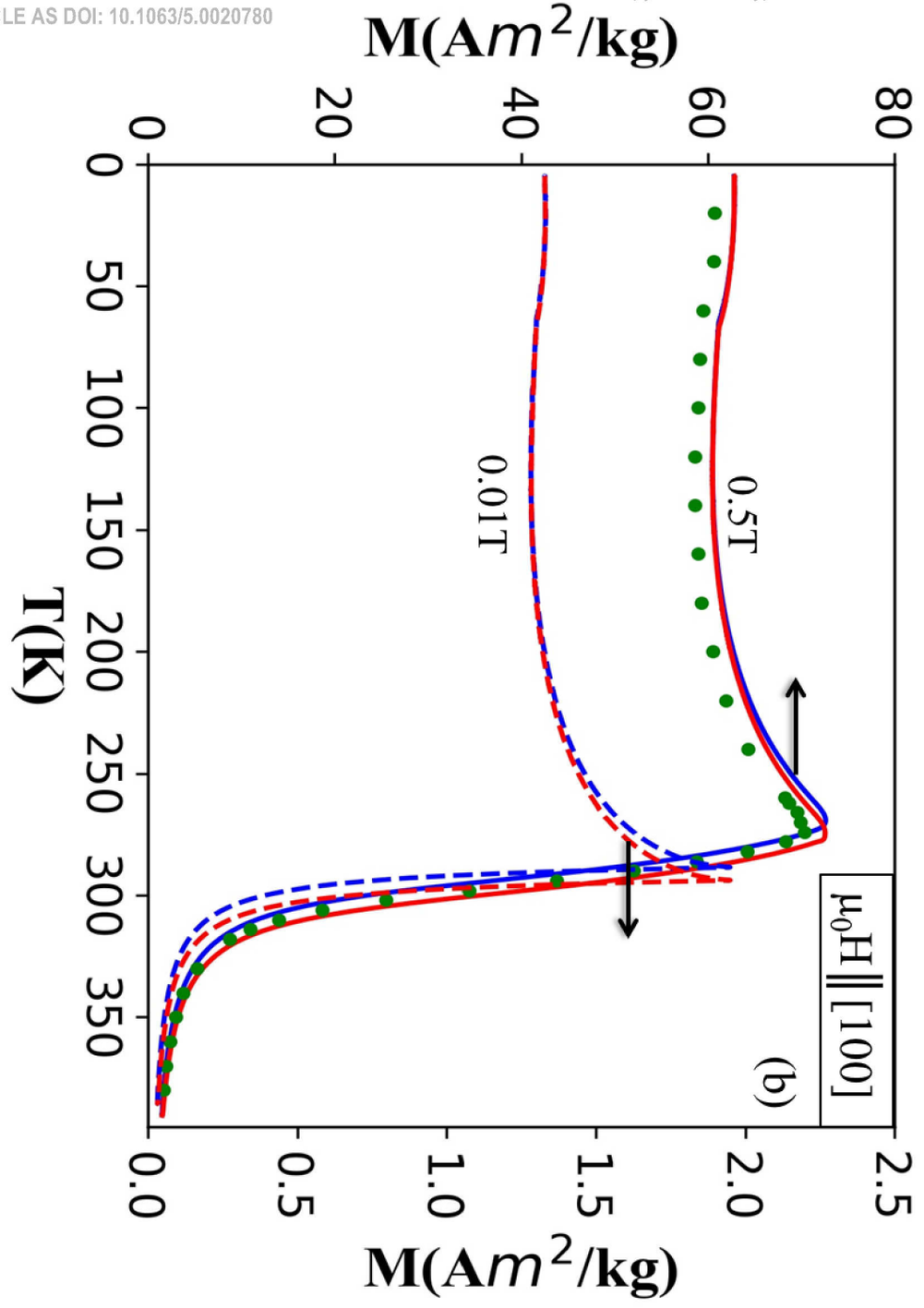

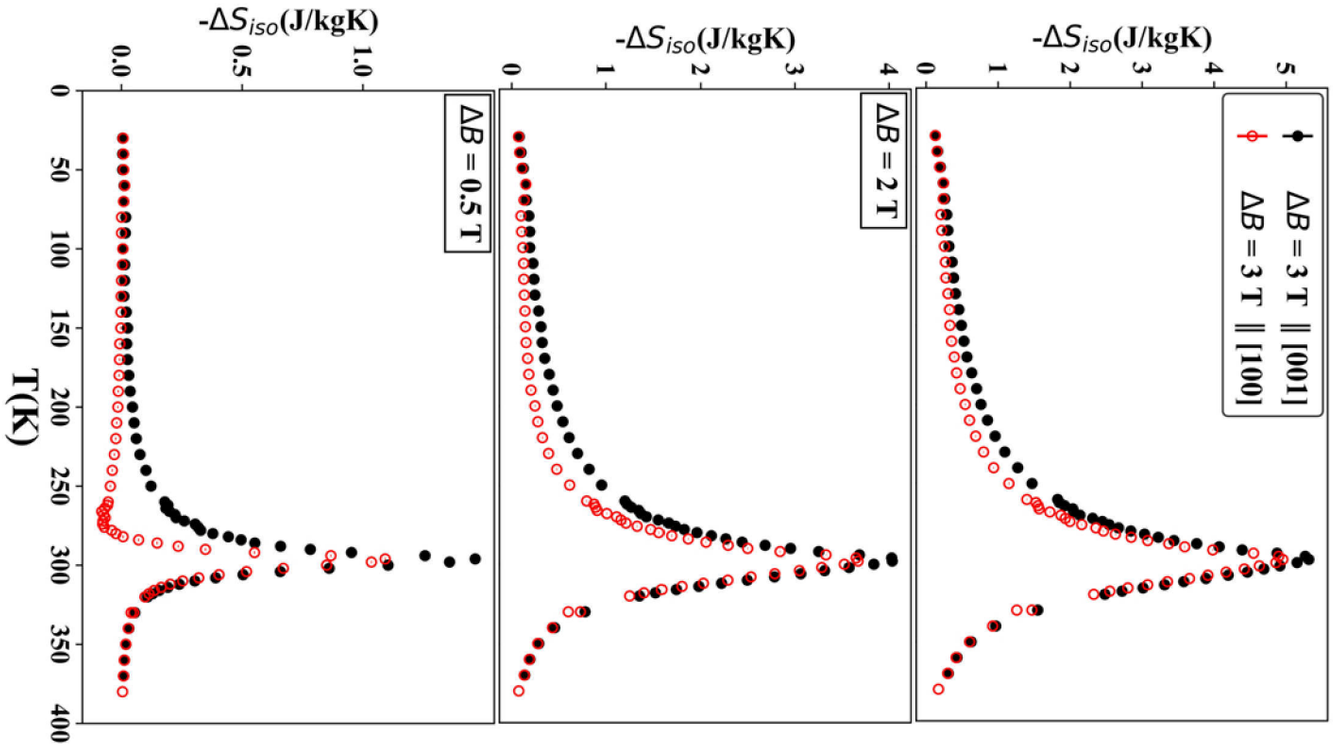

AIP Publishing

Journal of Applied Physics

ACCEPTED MANUSCRIPT

PLEASE CITE THIS ARTICLE AS DOI: 10.1063/5.0020780

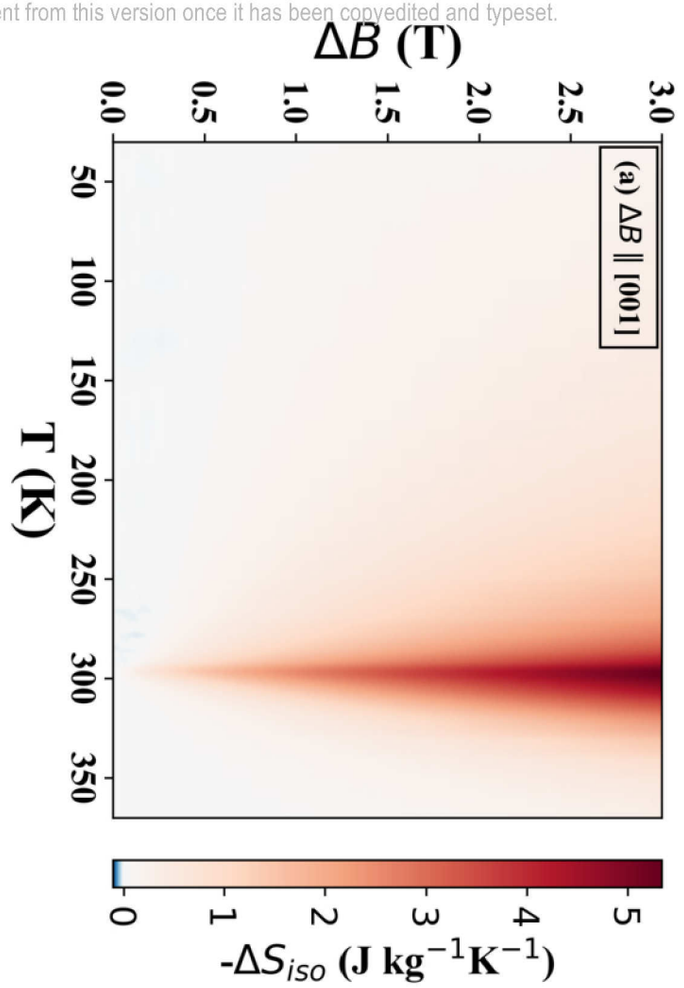

AIP Publishing

Journal of Applied Physics

ACCEPTED MANUSCRIPT

PLEASE CITE THIS ARTICLE AS DOI: 10.1063/5.0020780

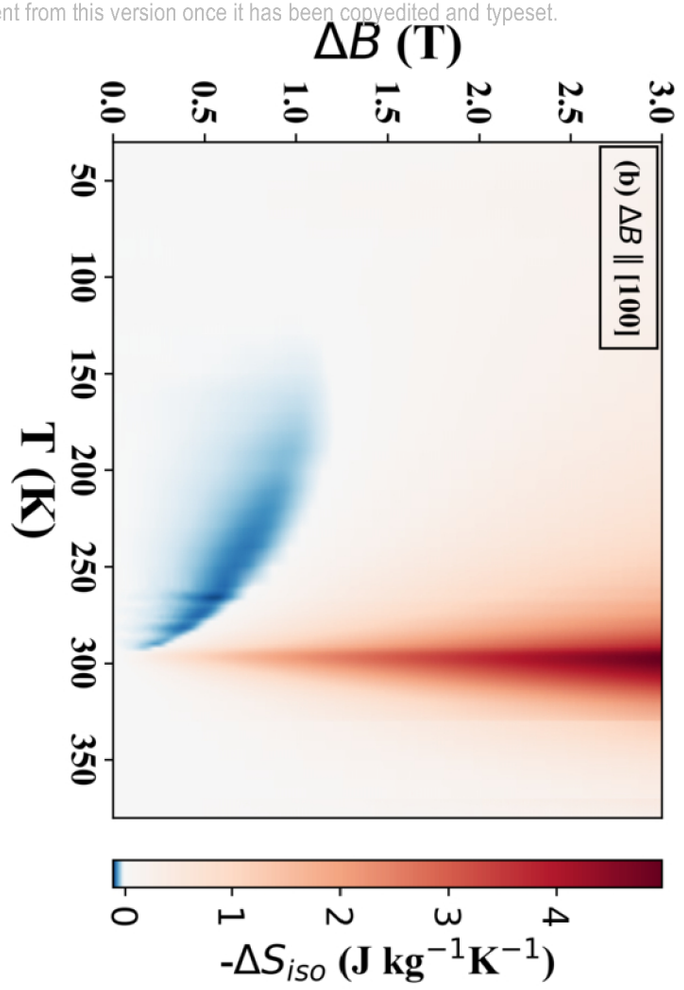

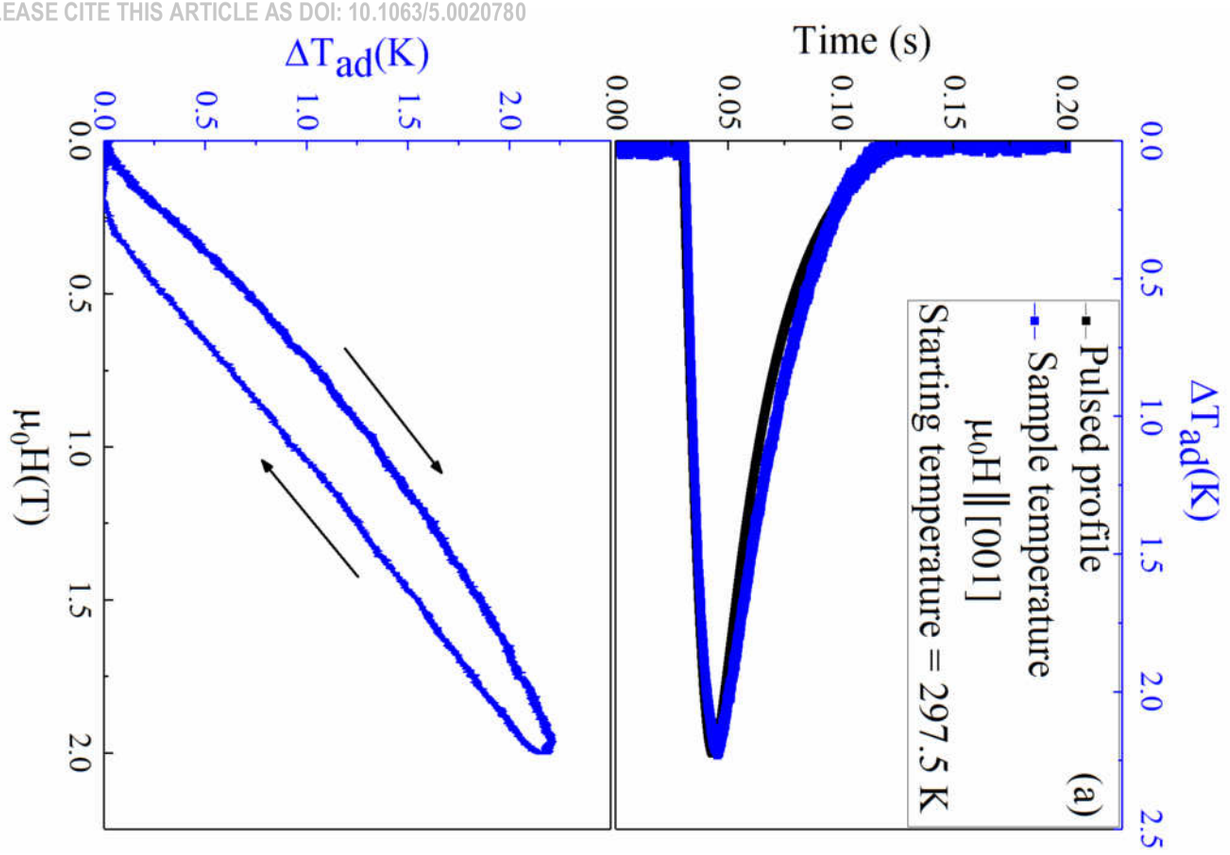

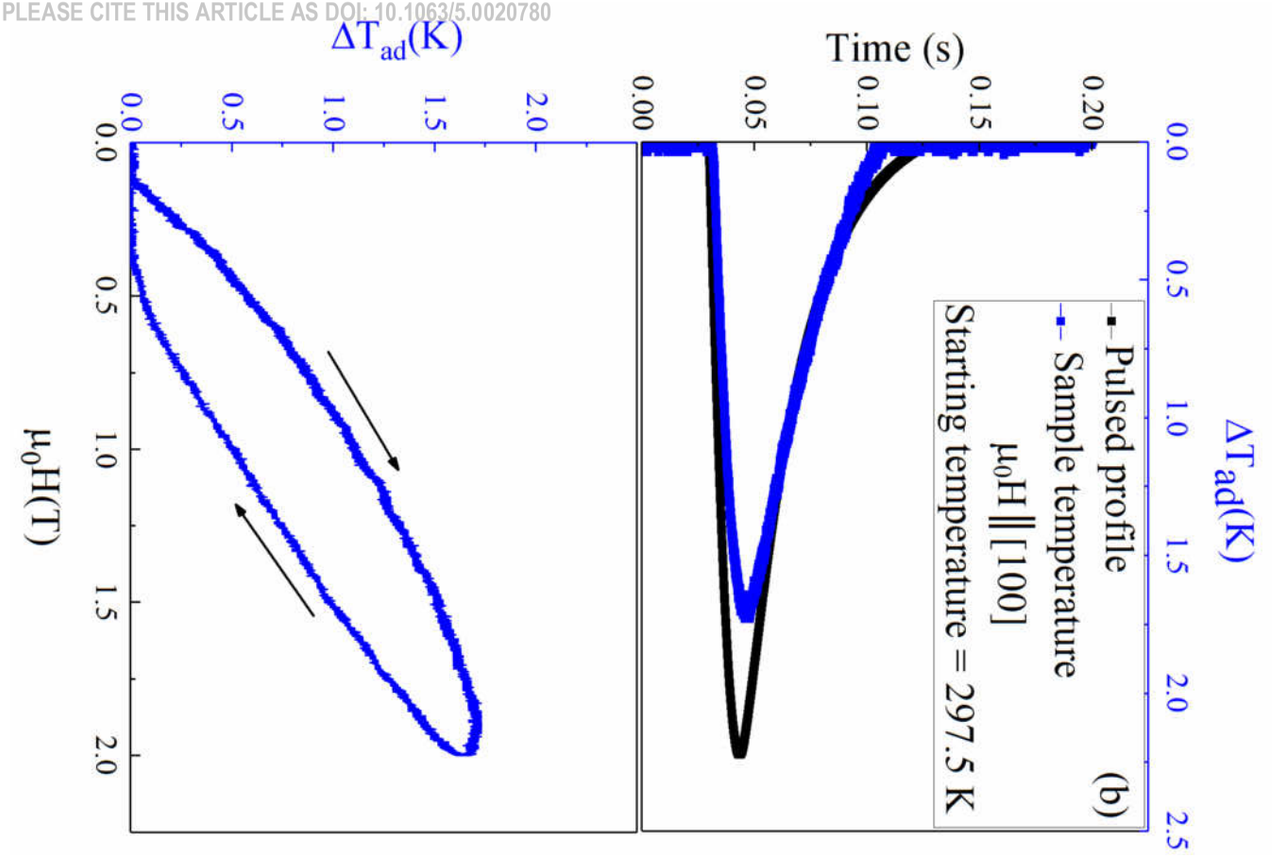

AIP Publishing
Journal of Applied Physics
ACCEPTED MANUSCRIPT

PLEASE CITE THIS ARTICLE AS DOI: 10.1063/5.0020780

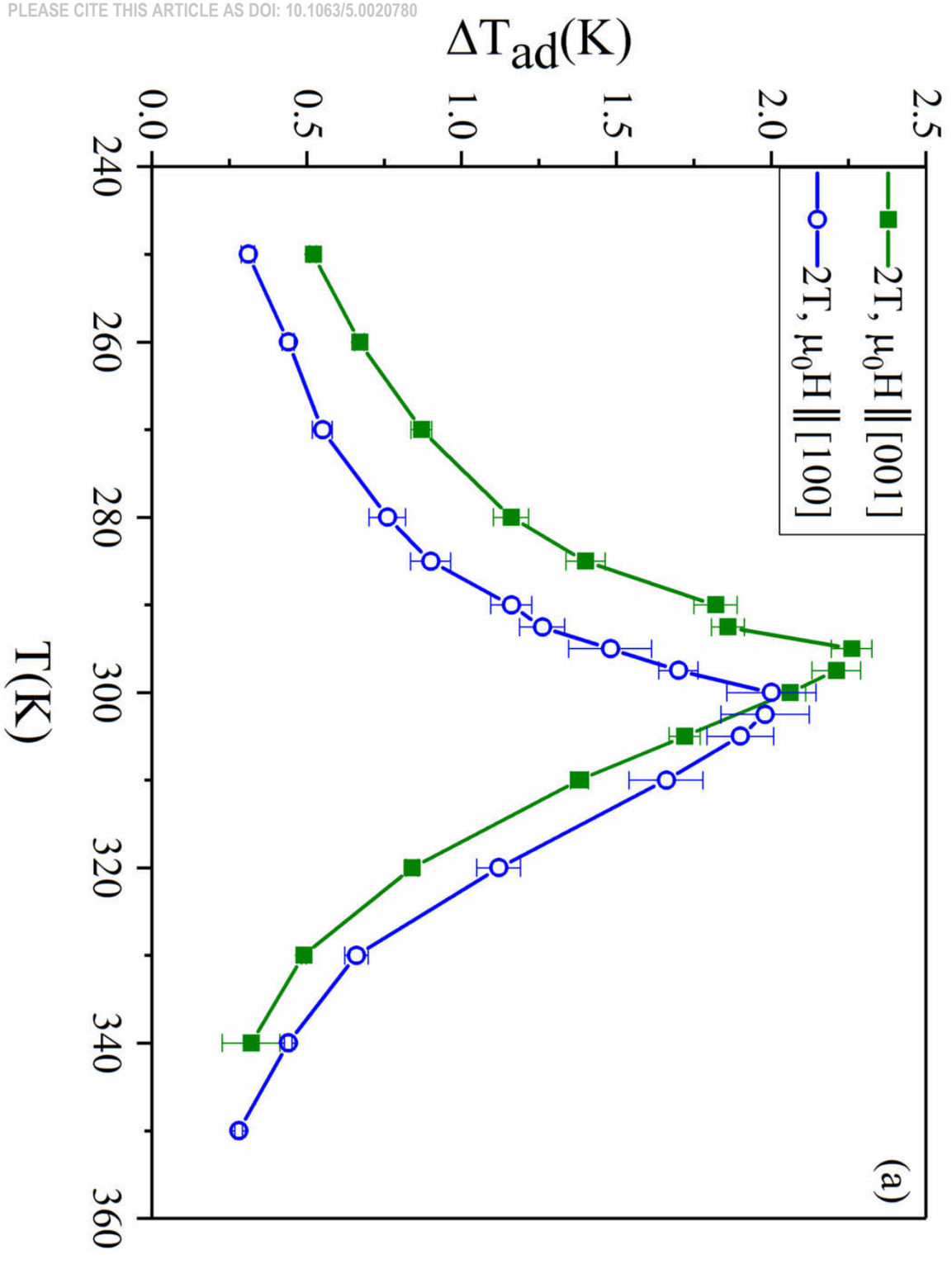

AIP Publishing
Journal of Applied Physics
ACCEPTED MANUSCRIPT

PLEASE CITE THIS ARTICLE AS DOI: 10.1063/5.0020780